

RESEARCH

Open Access



Adaptive neural network control of a centrifugal chiller system

Songchun Li¹ and M. Zaheeruddin^{1*}

Abstract

In this paper, a neuro-adaptive PI control strategy for a water-cooled centrifugal chiller system is developed, and its control performance is examined. The system model consists of a flooded evaporator, a flooded condenser, a centrifugal compressor, and an electronic expansion valve. The overall system consists of three control loops: a compressor speed control loop, an inlet guide vane (IGV) control loop, and a condenser liquid level control loop. A neuro-adaptive control strategy for compressor speed control was designed. The control performance of the chiller was tested by carrying out simulation runs using an integrated building and HVAC (IB-HVAC) system model. The major details of the IB-HVAC model are described in this paper. Results show that the neuro-adaptive controller can adapt to new system dynamics of the IB-HVAC system and give good setpoint tracking responses under a wide range of operating conditions. The results show that the neuro-adaptive controller performs better than the constant gain PI controller in terms of speed of response and setpoint tracking properties.

Keywords Centrifugal chiller, Compressor rotational speed, Neural network, Neuro-adaptive PI control, Cooling tower, Air handling units, Environmental zones

1 Introduction

Research conducted in the last decade shows that the energy savings associated with the operation of HVAC&R systems could be achieved mainly through two methods. Firstly, by installing variable speed drives on fans, compressors, and pumps and operating the system under variable fluid flow conditions, the fluid pumping costs could be reduced. Secondly, by implementing advanced control strategies on HVAC&R systems, improved operational performance and higher energy efficiency can be achieved. In this study, both objectives will be explored through the design and simulation of a neuro-adaptive control strategy for a variable-speed centrifugal chiller system.

In commercial buildings, the whole HVAC&R system consists of several subsystems such as cooling towers, chillers, air handling units, and environmental zones. Among these subsystems, the chiller system utilizes a considerable amount of energy to cool and dehumidify the air in the year-round air conditioning of buildings. To this end, there has been significant interest in improving the energy efficiency of chillers. In this study, a class of chiller system referred to as centrifugal chiller system is studied. The objective of this study is to develop a neuro-adaptive chiller control strategy to control the chilled water supply temperature against variable cooling loads acting on the system. The control performance of the chiller will be tested by conducting simulation runs under a wide range of operating conditions using an integrated building-HVAC system model.

With regard to control design and operation of HVAC systems, a review of the literature shows that PI/PID (proportional, integral, and derivative) controllers are the most popular controllers in the HVAC industry due to their simple structure and reliable control

*Correspondence:

M. Zaheeruddin
zaheer@encs.concordia.ca

¹ Building, Civil and Environmental Engineering, Concordia University, Montreal, Canada

performance. In practice, the PI/PID controller gains are set during the commissioning process. Normally, these gains are not altered during the operation; as a result, they do not perform well when the building load changes. To mitigate this issue, tuning methods are employed to update the controller gains. The Ziegler-Nichols tuning method described in reference [1] is widely used for tuning PI/PID controller gains. However, it was found that the PID controllers with constant gains do not perform well in systems with high non-linearity. To this end, several researchers found that the control performance could be improved by using self-tuning or adaptive PI/PID controllers. Both neural network and fuzzy logic-based adaptive controllers have been developed which reduce the overshoot and give good setpoint tracking performance.

Li and Zaheeruddin [2] developed a hybrid fuzzy logic controller by using two Sugeno types of fuzzy inference systems for a hot water district heating system. It was observed that the controllers with self-adaptive abilities provide a fast response and decrease overshoot. Pal and Mudi [3] developed a fuzzy logic-based self-tuning PI controller for supply air pressure control loop in an air conditioning and refrigeration system. Wu and Cai [4] developed an adaptive neuro-fuzzy method for controlling the supply air pressure in a HVAC system.

Zaheeruddin and Tudoroiu [5] developed a neuro-PID controller for controlling the discharge air temperature in air handling units (AHU). The simulation results showed that the control responses were smooth even when a large step change in the chilled water temperature was imposed as a disturbance on the system. In another study involving the applications of neural network controls, Ning [6] developed a model-based prediction and neural network optimization method, to design an optimal supervisory control algorithm for a two-zone VAV air conditioning system.

Zeng and Hu et al. [7] presented an adaptive neuro-PID controller for greenhouse climate control by using radial basis function network. The results demonstrate that the control strategy had strong robustness and good real-time performance.

In another study, Rasmussen and Alleyne [8] studied modeling and control of air conditioning and refrigeration systems. The study included simulation and experimental validation of the developed model of a vapor compression system suitable for control design. They proposed a gain-scheduled control approach to achieve high performance over the entire operating range.

Oliveira et al. [9] developed a switching control strategy for vapor compression refrigerators. Both compressor

speed and electronic expansion valve position control were investigated. The switching controller was shown to track the reference setpoint rapidly while rejecting imposed disturbances.

Sun and Wang [10] developed a control strategy for sequencing of multiple centrifugal chiller systems. The methodology uses online measurements and model predictions to improve energy efficiency. Along the same lines, Chang [11] proposed a method for maximizing the COP of the whole chiller plant, and the number of chillers required to match the cooling load.

The above review indicates that centrifugal chiller system operation in an integrated building and HVAC (IB-HVAC) system environment is not examined in detail. An IB-HVAC system is a network of four major subsystems, including a cooling tower, a chiller subsystem, air handling units, and the building. Each of these subsystems has its own local control loops. When the overall system operates in an IB-HVAC mode, the subsystem control loops must be designed in such a way that the effects of changes in cooling loads and the resulting dynamic interaction between the control loops are minimized. It is well known that the compressor, in a building cooling system, consumes substantial amount of energy, and as such, compressor control remains a challenging control problem due to its complex and nonlinear dynamics. To this end, it is important to develop improved compressor control strategies for efficient operation of chillers. Therefore, a major objective of this paper is to develop a neuro-adaptive PI (NAPI) control strategy for compressor speed control of a centrifugal chiller system. The focus will be to design a neural network-based adaptive controller which can adapt to temporal changes in cooling loads acting on the chiller system. The second objective of this study is to evaluate the NAPI controller performance in an integrated building and HVAC system simulation model. The goal is to maintain the overall IB-HVAC system operation smooth and stable as the NAPI compressor controller adapts to changes in system dynamics and control interactions over a wide range of operating conditions. The novelty of this approach is that only the compressor controller gains are updated adaptively while all the remaining control loops in the IB-HVAC system work with their respective well-tuned constant gain controllers. This simplifies the overall IB-HVAC system control for practical application. The basis for the NAPI control design is the set of data required for online simulation and training of the neural networks. For this purpose, the detailed centrifugal chiller model developed in a previous study by Li [12] was used. Here, a brief description of the chiller model is presented.

2 Centrifugal chiller model

The main components of the centrifugal chiller system (Fig. 1) consist of an evaporator, a condenser, a centrifugal compressor, and an electronic expansion valve. These components and flow direction of the fluids, including the water and the refrigerant loops, are depicted in Fig. 1.

The overall chiller system includes three control loops: (a) a compressor speed control loop, (b) an IGV control loop, and (c) a condenser liquid level control loop. Both compressor speed and IGV control are used to control the capacity of centrifugal chiller. In the compressor speed control mode, chilled water temperature is regulated at its setpoint by modulating input power (manipulated variable) to the compressor motor which changes the compressor rotational speed in response to variable cooling loads acting on the system. In IGV control mode, the chilled water temperature is controlled by manipulating the inlet guide vane position against variable cooling loads acting on the chiller. During the occupied periods, the compressor operates either in the compressor speed control mode or the IGV control mode. In the speed control mode, the IGV remains full-open, and the

compressor speed is modulated to maintain the chilled water supply temperature at its setpoint. As the required capacity decreases, the compressor speed decreases. When the compressor speed reaches its surge speed limit, the IGV control mode is activated, and the compressor speed is maintained at the surge speed.

The refrigerant liquid level in the condenser is controlled by manipulating the EXV opening in response to disturbances acting on the chiller system.

By applying the fundamental principles of mass, momentum, and energy balances, sets of equations for the component models and the overall chiller system model were developed in a previous study, and the model was validated with experimental data [12]. Here, a brief description of the model equations is given.

2.1 Flooded evaporator model

A flooded evaporator was divided into a two-phase section (TP) where the refrigerant is a mixture of liquid and vapor, and a superheat section (SH) where the refrigerant is superheated. Based on the energy and mass conservation principle, the heat exchanges between the chilled water and refrigerant are expressed by the following equations:

$$C_{chw,tp,1} \frac{dT_{chw,1}}{dt} = \dot{m}_{chw,tp,1} c_w (T_{chw,r} - T_{chw,1}) - N_{tb,ev,tp,1} U_{ev,tp} LMTD_{ev,tp,1} \tag{1}$$

$$C_{chw,tp,2} \frac{dT_{chw,sp,1}}{dt} = \dot{m}_{chw,tp,2} c_w (T_{chw,1} - T_{chw,sp,1}) - N_{tb,ev,tp,2} U_{ev,tp} LMTD_{ev,tp,2} \tag{2}$$

$$C_{chw,sh} \frac{dT_{chw,sp,2}}{dt} = \dot{m}_{chw,sh} c_w (T_{chw,1} - T_{chw,sp,2}) - N_{tb,ev,sh} U_{ev,sh} LMTD_{ev,sh} \tag{3}$$

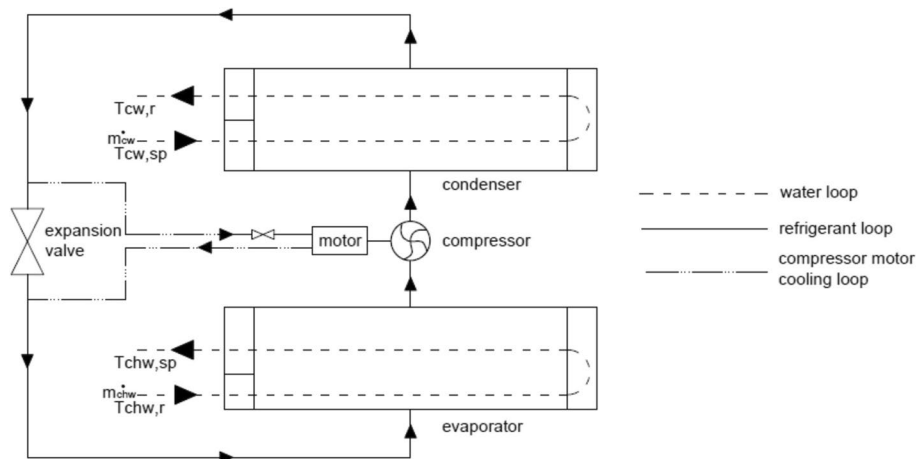


Fig. 1 Schematic diagram of a centrifugal chiller

$$T_{chw,sp} = \frac{N_{tb,ev,tp,2}T_{chw,sp,1} + N_{tb,ev,tp,1}T_{chw,sp,2}}{N_{tb,ev,tp,2} + N_{tb,ev,tp,1}} \quad (4)$$

$$C_{re,ev,sh} \frac{dT_{re,ev,out}}{dt} = N_{tb,ev,sh} U_{ev,sh} LMTD_{ev,sh} - \dot{m}_{re,ev} c_{p,re,v} (T_{re,ev,out} - T_{re,tp,ev}) \quad (5)$$

where $\dot{m}_{re,ev}$ is the refrigerant vapor generation rate in the evaporator, kg/s, which is calculated from Eq. (6).

$$\dot{m}_{re,ev} = \frac{N_{tb,ev,tp,1} U_{ev,tp,1} LMTD_{ev,tp,1} + N_{tb,ev,tp,2} U_{ev,tp,2} LMTD_{ev,tp,2}}{h_{fg,Pev}} + x_v (\dot{m}_{re,EXV} + \dot{m}_{re,motor}) \quad (6)$$

By assuming the density of the refrigerant vapor in the SH section is equal to the saturated vapor density at evaporation pressure as in Ning [6], a relationship between the evaporation pressure and the mass of the refrigerant inside the evaporator was established [12].

2.2 Flooded condenser model

The heat transfer between the refrigerant and the cooling water inside the condenser was described by the following dynamic equations:

$$C_{cw} \frac{dT_{cw,r}}{dt} = N_{tb,1,c} U_{tb,sh,c} LMTD_{sh,1,c} - \frac{2N_{tb,1,c}}{N_{total,c}} \dot{m}_{cw} c_w (T_{cw,r} - T_{cw,1}) \quad (7)$$

$$C_{cw} \frac{dT_{cw,sh}}{dt} = N_{tb,2,c} U_{tb,sh,c} LMTD_{sh,2,c} - \frac{2N_{tb,2,c}}{N_{total,c}} \dot{m}_{cw} c_w (T_{cw,sh} - T_{cw,sp}) \quad (8)$$

$$C_{cw} \frac{dT_{cw,tp}}{dt} = N_{tb,3,c} U_{tb,tp,c} LMTD_{tp,c} - \frac{2N_{tb,3,c}}{N_{total,c}} \dot{m}_{cw} c_w (T_{cw,tp} - T_{cw,sp}) \quad (9)$$

$$C_{cw} \frac{dT_{cw,sc}}{dt} = N_{tb,4,c} U_{tb,sc,c} LMTD_{sc,c} - \frac{2N_{tb,4,c}}{N_{total,c}} \dot{m}_{cw} c_w (T_{cw,sc} - T_{cw,sp}) \quad (10)$$

$$C_{cw} \frac{dT_{cw,1}}{dt} = N_{tb,2,c} U_{tb,sh,c} LMTD_{sh,2,c} + N_{tb,3,c} U_{tb,tp,c} LMTD_{tp,c} + N_{tb,4,c} U_{tb,sc,c} LMTD_{sc,c} - \frac{2(N_{tb,2,c} + N_{tb,3,c} + N_{tb,4,c})}{N_{total,c}} \dot{m}_{cw} c_w (T_{cw,1} - T_{cw,sp}) \quad (11)$$

$$C_{re,sc} \frac{dT_{re,sc,c}}{dt} = (\dot{m}_{re,EXV} + \dot{m}_{re,motor}) c_{p,Re,l,c} (T_{re,tp,c} - T_{re,sc,c}) - N_{tb,4,c} U_{tb,sc,c} LMTD_{sc,c} \quad (12)$$

2.3 Centrifugal compressor model

The percent volumetric flow Θ and the percent head of the refrigerant through the compressor are modeled using the method described in ASHRAE Handbook [13] for the case when the inlet guide vane is in “wide-open-vane” position.

$$\Omega = \mu(V_p^2/a^2) \tag{13}$$

$$\Theta = \frac{V_p}{a\pi} \frac{\dot{Q}}{U_{com}N_{com}D^3} \tag{14}$$

where U_{com} is the control input to the compressor speed controller, which is used to control the chilled water supply temperature. In addition, the polytropic efficiency (Korpela [14]), the polytropic compression work (Bendapudi and Braun [15]) per unit mass of refrigerant, and the motor efficiency (Wong and Wang [16]) were modeled using the approach cited in the above references:

$$\eta_p = \left(\frac{n-1}{n}\right)\left(\frac{\gamma}{\gamma-1}\right) \tag{15}$$

$$W_p = \left(\frac{P_{disc}}{P_{re,disc}} - \frac{P_{suc}}{P_{re,suc}}\right) \frac{\ln(P_{disc}/P_{suc})}{\ln[(P_{disc}P_{re,suc})/(P_{suc}P_{re,disc})]} \tag{16}$$

$$\eta_{motor} = \alpha_1 + \alpha_2(PLR) + \alpha_3(PLR)^2 \tag{17}$$

From the above equations, the total electrical power input to the compressor is computed from the following equation.

$$P_{elec} = \frac{\dot{m}_{re,com}W_p}{\eta_p\eta_{motor}} \tag{18}$$

2.4 Electronic expansion valve (EXV) model

The mass flow rate of refrigerant through EXV was modeled as a function of opening area as described in Yu and Chan [17].

$$\dot{m}_{re,EXV} = U_{EXV}C_dA_{EXV,max}\sqrt{2(P_c - P_{ev})\rho_{re,c,out}} \tag{19}$$

The enthalpy of the refrigerant entering the evaporator is computed from:

$$h_{re,ev,in} = \frac{\dot{Q}_{motor}}{cf \cdot \dot{m}_{re,com}} + h_{re,c,out} \tag{20}$$

Based on operating experience, “cf” in Eq. (20) is normally set to 0.15. This implies that 15% of the refrigerant is used to cool the compressor motor.

3 Neuro-adaptive PI control strategy

The literature review indicates that most researchers employed regression techniques to develop data-driven chiller models. However, according to Zaheeruddin et al. [5], the neural network models are more accurate and robust, which makes them attractive candidates for

the design of control strategies for highly nonlinear centrifugal chiller systems. Therefore, in this study, a neuro-adaptive PI (NAPI) controller will be developed for the centrifugal chiller system. Furthermore, in the multi-mode operation of chiller systems, energy savings are mainly achieved during compressor speed control mode. To this end, a NAPI controller is developed for speed control of the chiller system. The IGV and EXV control loops were operated with constant gain PI controllers.

3.1 Design of a neuro-adaptive PI controller for centrifugal chiller

In a previous study [12], it was demonstrated that the COP of chillers is significantly affected by the partial load ratio *PLR*, the chilled water supply temperature, and the condenser cooling water supply temperature. The results indicated that the chiller COP could be increased by increasing the chilled water supply temperature $T_{chw,sp}$, by decreasing the cooling water supply temperature $T_{cw,sp}$ or by employing both options. Under partial cooling load conditions such as when the zones are unoccupied, energy savings could be achieved by increasing the chilled water supply temperature without affecting the thermal comfort conditions of the space. In other words, by operating the chiller under compressor speed control mode, it is possible to regulate the temperature of chilled water and thus save energy in response to the cooling loads acting on the system. Also, further energy savings can be achieved by using optimal chilled water supply temperature $T_{chw,sp}$ setpoints for control of chiller systems.

Once the optimal chilled water supply temperature setpoints are determined, it will be important to design a good controller to track the optimal setpoints as accurately as possible. In this regard, a neuro-adaptive PI controller is a preferred option due to highly nonlinear dynamics of the chiller system. Therefore, a neuro-adaptive PI controller will be developed to modulate the chiller speed for regulating the chilled water supply temperature $T_{chw,sp}$.

The architecture of NAPI controller proposed in this study is depicted in Fig. 2. In Fig. 2, the chiller system is operated in a compressor speed control mode while the IGV control remains in full-open position. A neural network structure consisting of 3 layers, namely 3–2–1, was used. By using the error back propagation algorithm and the input–output data set generated through simulation runs, the feed-forward neural network was trained. The training was continued until the mean square root error criterion is met. After the initial training, the neural network was then linked to the centrifugal chiller plant model, and simulations were conducted in an online

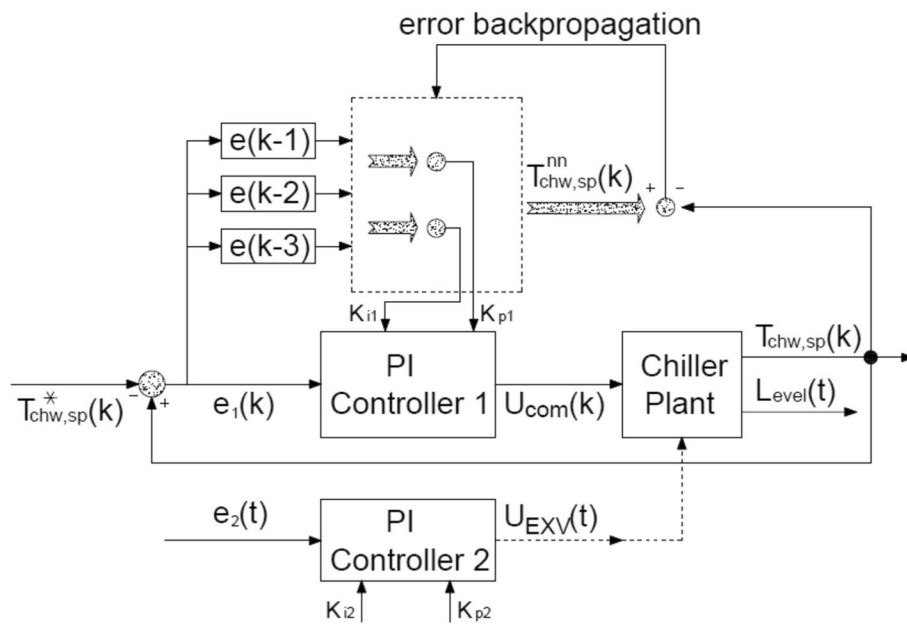


Fig. 2 Neuro-adaptive PI controller for the centrifugal chiller

adaptive control mode. The hidden layer outputs of the neural network are the PI controller-1 gains k_{p1} and k_{i1} shown in Fig. 2. The controller gains are continuously updated to maintain the chilled water supply temperature $T_{chw,sp}$ close to a desired setpoint.

The gains k_{p2} and k_{i2} for the PI controller-2 were obtained by using the Ziegler-Nichols tuning method [1]. Since the refrigerant liquid level setpoint is constant, the gains k_{p2} and k_{i2} obtained from the initial tuning were found to give good control performance. The control input signal for the centrifugal compressor speed U_{com} is calculated based on the gain values k_{p1} and k_{i1} , and likewise the EXV opening U_{EXV} is calculated based on the gain values k_{p2} and k_{i2} , using the current error and the accumulated error between the control variables and their respective setpoints.

The weights and the bias of the hidden layer are updated through the error back propagation method by comparing the output of the chiller plant $T_{chw,sp}$ and the output of the neural network $T^{nn}_{chw,sp}$. The gain values k_{p1} and k_{i1} were continuously updated during the online operation. Also, the error between the chiller plant output $T_{chw,sp}$ and the target value $T^*_{chw,sp}$ are calculated, in which, the current step error $e(k)$ is the input for the PI controller-1, and the past 3 step errors $e(k - 1)$, $e(k - 2)$, $e(k - 3)$ are the inputs for the neural network. From the simulation runs, it was found that the neural network converges faster when the past 3 step errors are fed as inputs during online training.

The main objective of the NAPI control strategy is to let the neural network learn and adapt to the load changes online and update the PI controller gains k_p and k_i for compressor speed control. Thus, the centrifugal chiller speed is controlled online to maintain the chilled water supply temperature at its setpoint.

3.2 Neuro-adaptive PI controller performance–simulation results

In this simulation, a variable setpoint profile for the chilled water supply temperature (target value for the neural network $T^*_{chw,sp}$) is assumed. The chilled water supply temperature setpoint was set at $T^*_{chw,sp} = 44$ °F for the first 8000 s (2.2 h), $T^*_{chw,sp} = 49$ °F for the next 4000 s (1.1 h), and $T^*_{chw,sp} = 44$ °F for the last 6000 s (1.7 h) of the simulation time horizon of 5 h as shown in Fig. 3h. In the simulation runs, both the chilled water return temperature $T_{chw,r}$ (Fig. 3c) and the cooling water supply temperature $T_{cw,sp}$ (Fig. 3d) were maintained constant at 54 °F and 85°F, respectively. The resulting tracking responses of the NAPI controller due to this change in setpoint of chilled water supply temperature are depicted in Fig. 3a–g, i, j.

The cooling capacity of the compressor (Fig. 3e) is higher in the first 2.2 h in response to lower chilled water supply temperature setpoint (44 °F in Fig. 3h) followed by lower compressor capacity when the chilled water setpoint is increased to 49 °F. In other words, the NAPI controller is modulating the compressor speed (Fig. 3g)

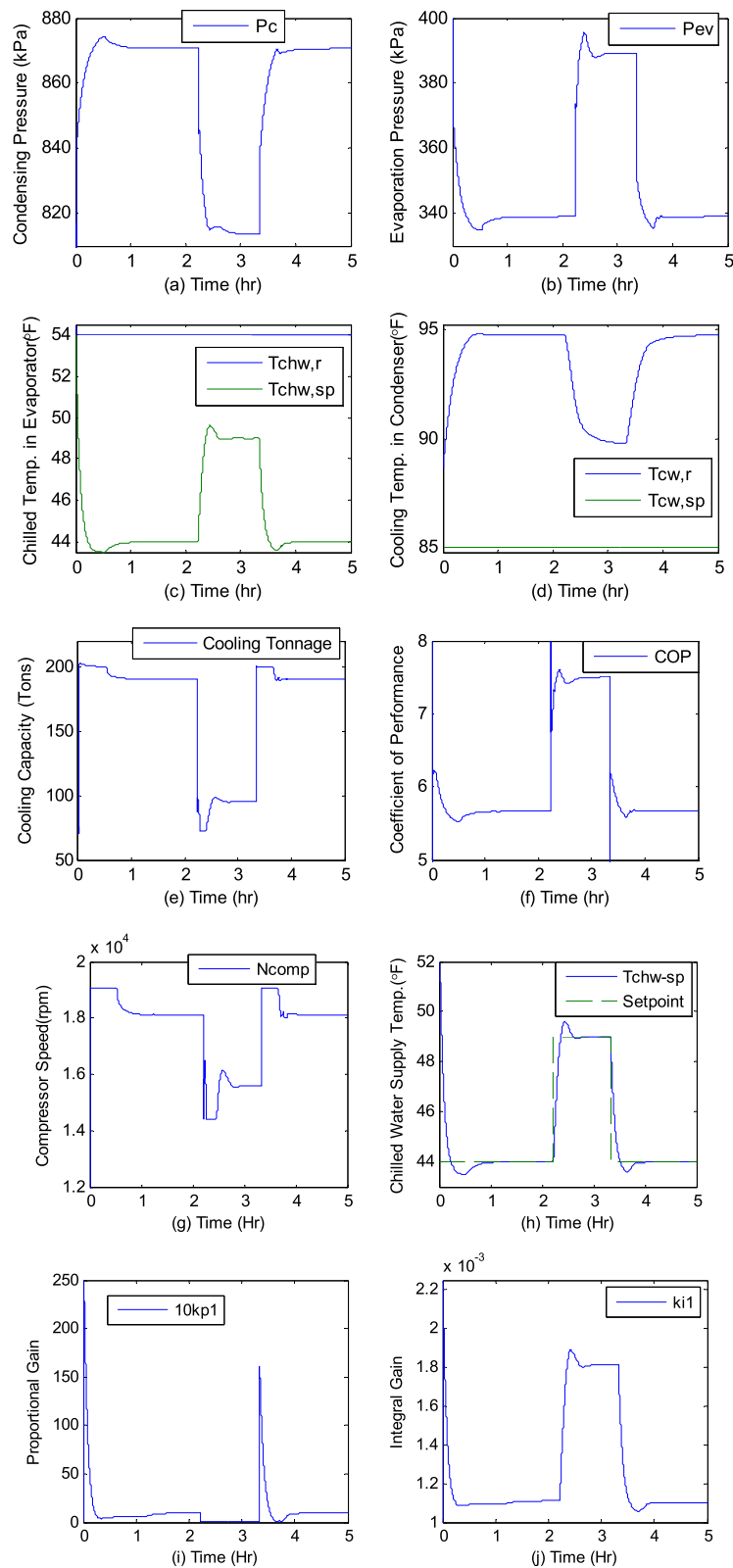


Fig. 3 Responses of the centrifugal chiller with neural network adaptive PI controller

to track the higher and lower loads imposed on the compressor via the setpoint changes in chilled water supply temperature. Therefore, the overall responses of the system in Fig. 3a–j reflect the high and low load responses as a function of chilled water supply temperature setpoint profile chosen for this simulation (Fig. 3h).

It is also worth noting the fact that when the chiller runs at near full capacity (nominal capacity) as shown in Fig. 3e, the COP is lower as depicted in Fig. 3f. And when the chiller capacity decreases, the COP is higher (Fig. 3f).

The simulation results depicted in Fig. 3h show that the NAPI controller reveals a good tracking performance, including zero steady-state error, and good transient behavior when subjected to a sudden change in the setpoint and the overshoot remained less than 0.5 °F. In addition, from Fig. 3i, j, it can be noted that after the initial transients, the proportional gain k_p and the integral gain k_i reach near constant values under steady-state conditions. As the chilled water supply temperature setpoint is increased, the proportional gain decreases rapidly to reduce the control input signal to the compressor thereby reducing the compressor speed, and consequently, the refrigerant mass flow rate is decreased which increases the chilled water temperature to reach the new setpoint.

3.3 Comparison between the constant gain PI and neuro-adaptive PI control responses

To compare the control performance of the centrifugal chiller system with the constant gain PI controller and the neuro-adaptive PI controller, simulation runs were made using a PI controller with constant gains ($k_{p1} = 0.5$, and $k_{i1} = 0.006$) while keeping the operating conditions similar to those of the NAPI controller. The results are shown in Fig. 4a–h.

From Figs. 3 (NAPI control) and 4 (constant gain PI control), it is apparent that the centrifugal chiller system responses show similar trends. However, from Figs. 3h and 4h, it is evident that the neuro-adaptive PI controller has better tracking control performance than the constant gain PI controller, in that it reaches the new setpoint much faster, and the overshoot is much smaller. The constant gain PI controller takes twice as long as the NAPI controller to reach a new steady state when the supply water temperature setpoint is increased by 5 °F.

4 Implementation of NAPI control in an integrated building-HVAC system model

The results presented in Fig. 3 reveal that the proposed neural network adaptive PI control strategy offers advantages in both setpoint tracking and smooth responses over the conventional PI control strategy. However, the data used for training is unlikely to cover all possible operating scenarios. In other words, the proposed neural network adaptive PI control strategy may not work well for cases other than for which it is trained, unless it learns and adapts online to new system dynamics. To verify the robustness of the control strategy to learn and adapt to new system dynamics, the NAPI control was implemented in an integrated building-HVAC (IB-HVAC) system model, and simulation runs were made under real weather data and typical building operating conditions.

5 The IB-HVAC system model

The integrated building and HVAC (IB-HVAC) system model depicted in Fig. 5 was utilized as a simulation test bench for studying the performance of HVAC systems and control strategies. The entire system comprises a cooling tower, two air handling units (AHUs), two zones, and the centrifugal chiller, which is the test unit of the IB-HVAC system. In the following the IB-HVAC system model equations are presented.

By applying the fundamental principles of mass, momentum, and energy balances, the component models for the cooling tower, centrifugal chiller, AHUs, and the environmental zones were developed. The component models were then interconnected with proper boundary conditions to develop the overall model of the IB-HVAC system.

6 The cooling tower model

The cooling tower is a heat dissipation equipment which is used to cool the warm water from the condenser. The water exchanges heat with the air by convection in a direct contact process. The mass transfer between the liquid water film on the surface of the tower fill and the flowing air occurs. To model the heat transfer processes in the cooling tower, the cooling tower is divided into several elements evenly spaced over the total volume of the fill material (Fig. 6). By assuming one-dimensional heat transfer, the energy balance and water vapor mass balance equations for each element (i) were derived.

$$U_{CT} \dot{m}_{a,CT} (h_i - h_{i-1}) = h_C (T_{w,i} - T_{a,i}) + h_D (w_{sat,T_{w,i}} - w_i) h_{fg,T_{w,i}} \quad (21)$$

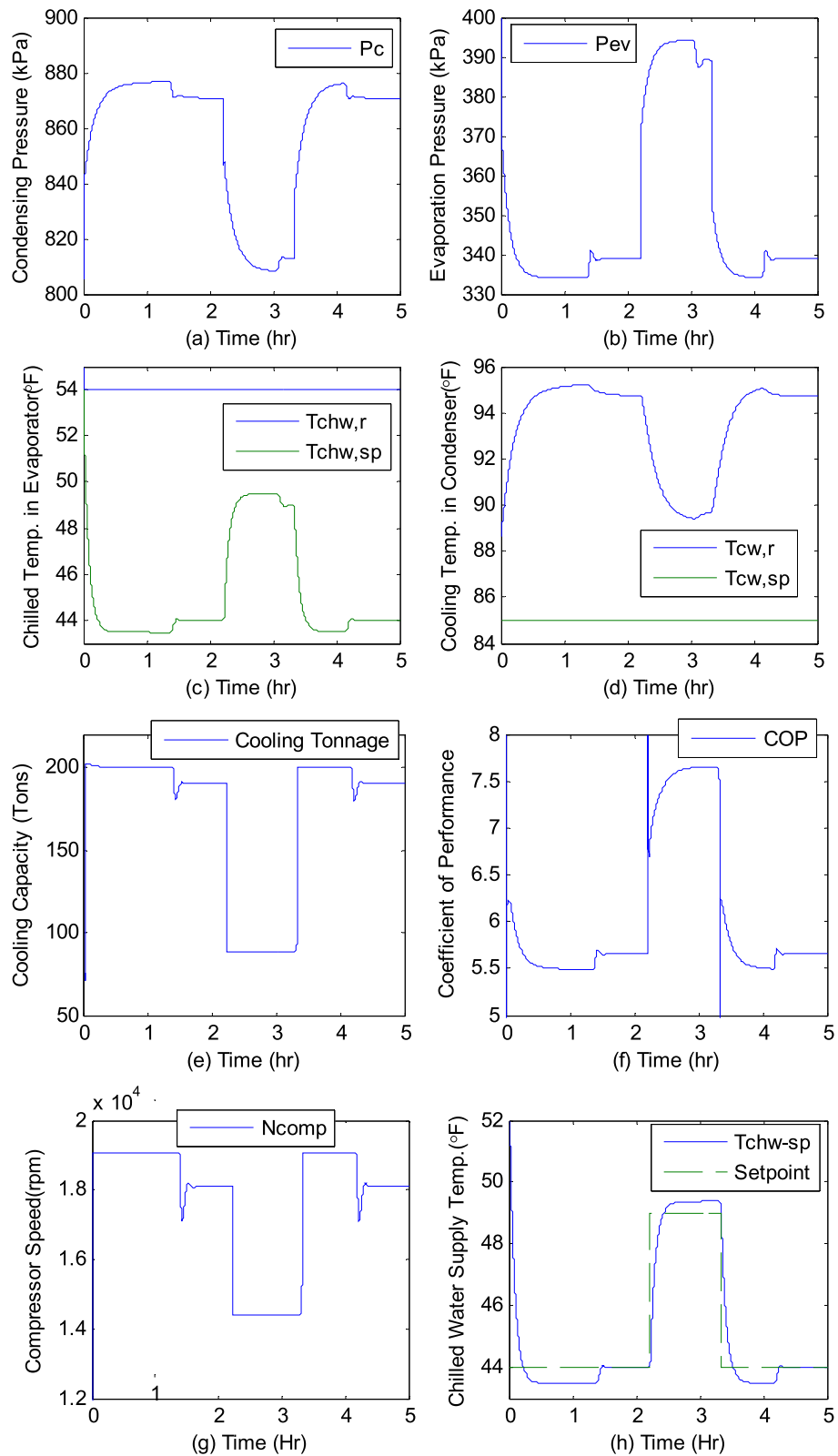


Fig. 4 Responses of the centrifugal chiller with constant gain PI controller

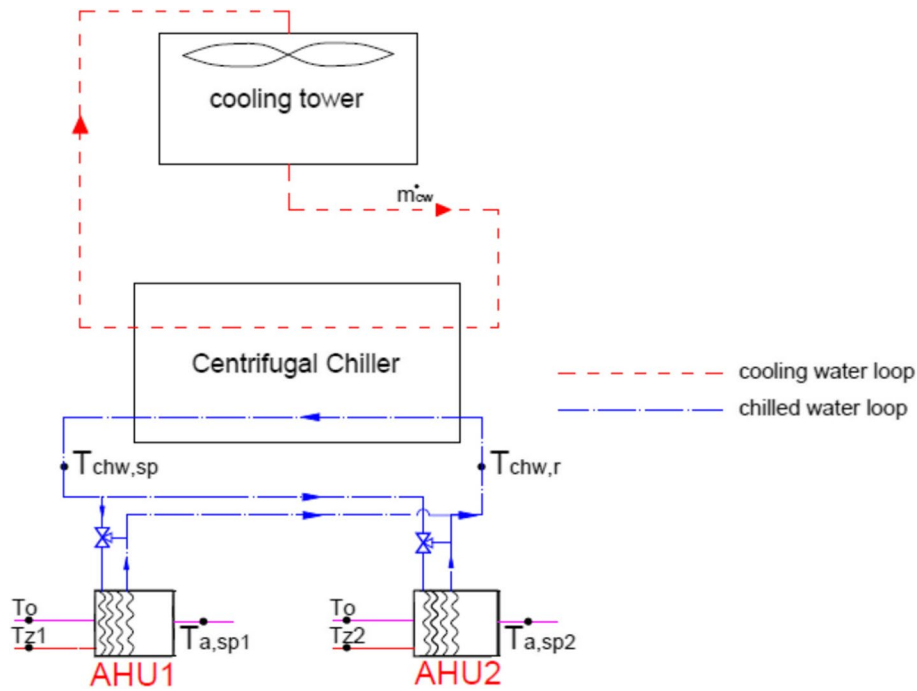


Fig. 5 Schematic diagram of IB-HVAC system with centrifugal chiller

$$w_i = w_{i-1} + \frac{h_D(w_{sat,T_{w,i}} - w_i)}{U_{CT} \dot{m}_{a,CT}} \quad (22)$$

$$C_{w,i,CT} \frac{dT_{w,i}}{dt} = \dot{m}_{w,i+1} c_w T_{w,i+1} - \dot{m}_{w,i} c_w T_{w,i} - h_C(T_{w,i} - T_{a,i}) - h_D(w_{sat,T_{w,i}} - w_i) h_{fg,T_{w,i}} \quad (23)$$

$$\dot{m}_{w,i} = \dot{m}_{w,i+1} - h_D(w_{sat,T_{w,i}} - w_i) \quad (24)$$

$$h_i = 1.01 T_{a,i} + (2500 + 1.84 T_{a,i}) w_i \quad (25)$$

where U_{CT} is the control input to the cooling tower fan motor, which varies between 0 and 1. The control signal U_{CT} modulates the fan speed to maintain the cooling tower water temperature $T_{w,1}$ close to the setpoint.

7 Centrifugal chiller model

The model Eqs. (1–20) for the centrifugal chiller were described in the earlier section on centrifugal chiller model. The chiller performance with the NAPI control

strategy will be tested by conducting a typical day simulation of the IB-HVAC system.

8 Modeling of air handling units (AHUs)

The AHU cooling coils were modeled by using the finite control volume method. Each row of the tubes (Fig. 7) is assumed as a control volume, and the energy and mass balance principle is applied to derive a set of equations for the air temperature $T_{a,AHU,k}$ and the chilled water temperature. The subscript k refers to the row number of the tubes in each AHU, and $T_{a,AHU,0}$ is the supply air temperature entering the cooling coil which is the mixed air (outdoor and recirculated air) temperature. $T_{w,AHU,k+1}$ is the chilled water supply temperature to the cooling coil. The set of equations are given below.

$$C_{a,AHU,k} \frac{dT_{a,AHU,k}}{dt} = U_{asp,AHU} \dot{m}_{aspd,AHU} c_a (T_{a,AHU,k-1} - T_{a,AHU,k}) - N_{tube,AHU} U_{a-tw,AHU} LMTD_{a-tw,AHU,k} \quad (26)$$

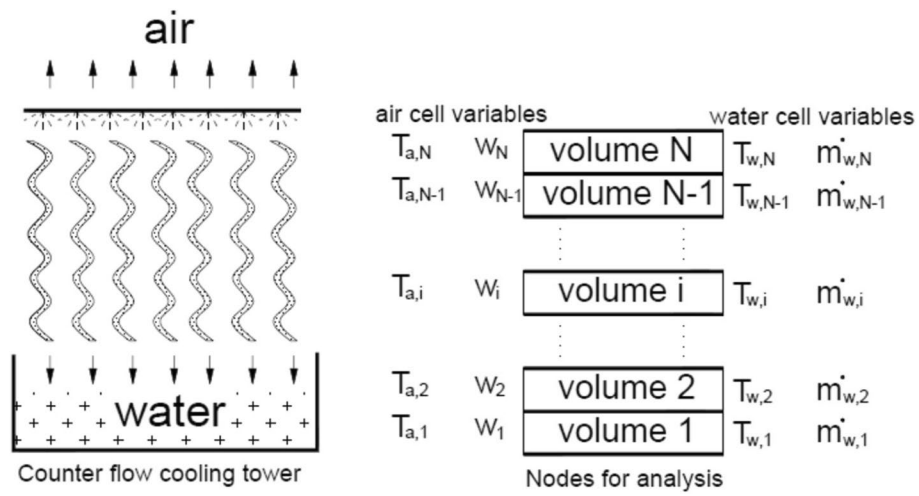


Fig. 6 Schematic diagram of the cooling tower

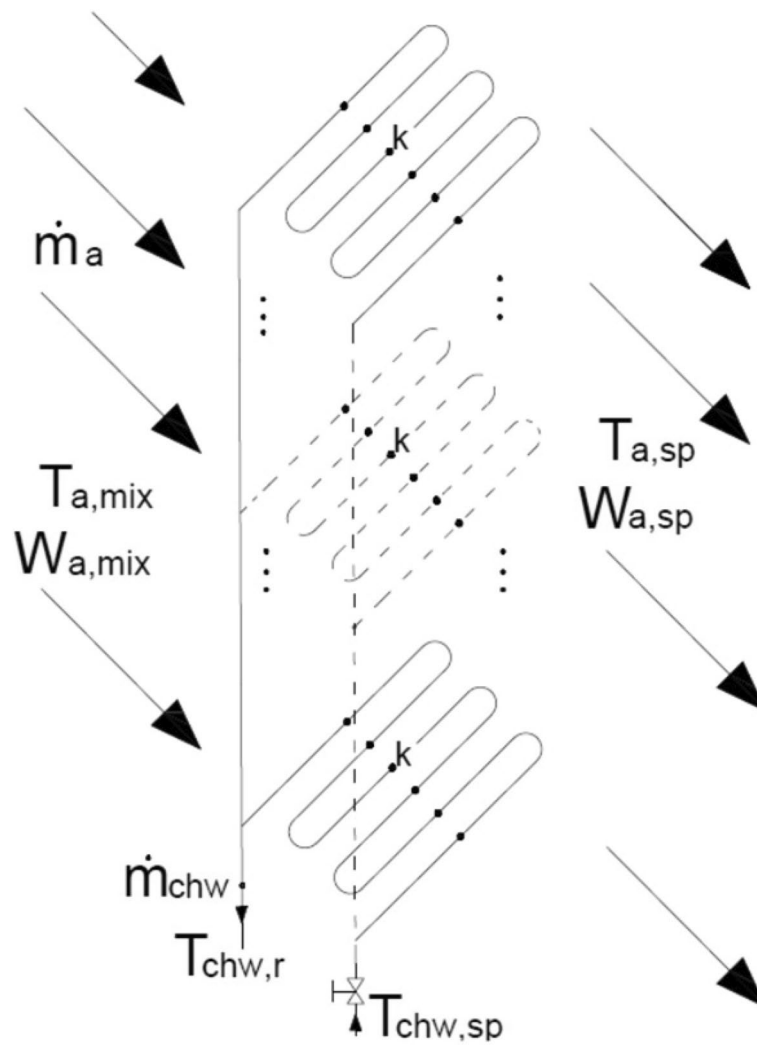


Fig. 7 Configuration of the cooling coils

$$C_{tw,AHU,n,k} \frac{dT_{w,AHU,n,k}}{dt} = N_{tube,AHU,n} (U_{a-tw,AHU,n} LMTD_{a-tw,AHU,n,k} - U_{tw-w,AHU,n} LMTD_{tw-w,AHU,n,k}) \tag{27}$$

$$C_{w,AHU,n,k} \frac{dT_{w,AHU,n,k}}{dt} = N_{tube,AHU,n} U_{tw-w,AHU,n} LMTD_{tw-w,AHU,n,k} + \dot{W}_{cond,AHU,n,k} h_{fg} - U_{chw,n} \dot{m}_{wd,AHU,n} c_w (T_{w,AHU,n,k} - T_{w,AHU,n,k+1}) \tag{28}$$

$$\dot{W}_{cond,AHU,n,k} = h_{D,AHU} A_{o,tube,AHU,n} N_{tube,AHU,n} \eta_{fin} (W_{sat@T_{tw,AHU,n,k}} - W_{a,AHU,n,k}) \tag{29}$$

$$U_{asp,AHU,n} \dot{m}_{aspd,AHU,n} \frac{dW_{a,AHU,n,k}}{dt} = U_{asp,AHU,n} \dot{m}_{aspd,AHU,n} W_{a,AHU,n,k-1} - \dot{W}_{cond,AHU,n,k} \tag{30}$$

In the above equations, the chilled water flow rate $U_{chw,AHU,n}$ in the air handling unit n is normalized and ranges between 0 and 1. The chilled water flow rate is modulated to regulate the discharge air temperature $T_{a,AHU,n,k}$ which is also the supply air temperature to the zones. The returned chilled water temperature to the chiller is determined by using Eq. (31).

$$T_{chw,r} = \frac{\sum_{n=1,2,3,\dots,n} \{[(1 - U_{chw,AHU,n})T_{chw,sp} + U_{chw,AHU,n}T_{w,AHU,n,k+1}] \dot{m}_{wd,AHU,n}\}}{\sum_{n=1,2,3,\dots,n} (\dot{m}_{wd,AHU,n})} \tag{31}$$

9 Zone model

The heat transfer from the exterior elements of the zones, the composite walls, and the roof were modeled using the finite difference method. Standard wall and roof construction types (Fig. 8) described in ASHRAE load calculation manual [13] were used. To reduce the complexity of the model, the temperature of each layer of the composite wall and roof (Fig. 8) is assumed to be uniform, and the heat transfer is one-dimensional along the depth. The equations for interior nodal surface temperatures of the north-, south-, east-, and west-facing walls and the roof were developed.

For zone i , the temperature nodes are $T_{bri,1,zi,j}$ (1st half of the brick layer), $T_{bri,2,zi,j}$ (2nd half of the brick layer), and $T_{plas,zi,j}$ (plaster board layer) of the external wall facing each direction j (j represents south, north, east, and west, respectively). Similarly, for the roof the temperature nodes are $T_{mor,1,zi}$ (1st half of the mortar layer), $T_{mor,2,zi}$ (2nd half of the mortar layer), $T_{crt,1,zi}$ (1st half of the concrete layer), $T_{crt,2,zi}$ (2nd half of the concrete layer), and $T_{plas,zi}$ (plaster board layer). The dynamic equations

describing the heat transfer processes through the walls and roof were written. These are,

$$C_{bri,1,zi,j} \frac{dT_{bri,1,zi,j}}{dt} = \alpha A_{w,zi,j} I_{solar,j} + U_{o,bri1} A_{w,zi,j} (T_o - T_{bri,1,zi,j}) - U_{bri1,bri2} A_{w,zi,j} (T_{bri,1,zi,j} - T_{bri,2,zi,j}) \tag{32}$$

$$\frac{dT_{bri,2,zi,j}}{dt} = \frac{A_{w,zi,j}}{C_{bri,2,zi,j}} [U_{bri1,bri2} (T_{bri,1,zi,j} - T_{bri,2,zi,j}) - U_{bri2,plas} (T_{bri,2,zi,j} - T_{plas,zi,j})] \tag{33}$$

$$\frac{dT_{plas,zi,j}}{dt} = \frac{A_{w,zi,j}}{C_{plas,zi,j}} [U_{bri2,plas} (T_{bri,2,zi,j} - T_{plas,zi,j}) - U_{plas,z} (T_{plas,zi,j} - T_{zi})] \tag{34}$$

$$C_{mor,1,zi} \frac{dT_{mor,1,zi}}{dt} = \alpha A_{r,zi} I_{solar,H} + U_{o,mor1} A_{r,zi} (T_o - T_{mor,1,zi}) - U_{mor1,mor2} A_{r,zi} (T_{mor,1,zi} - T_{mor,2,zi}) \tag{35}$$

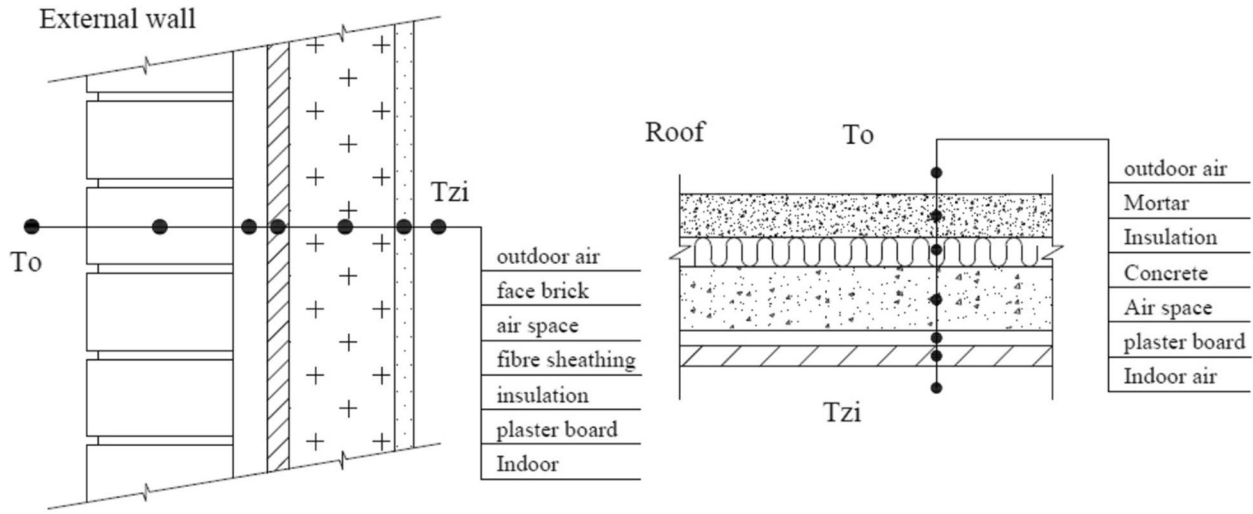


Fig. 8 The external walls and roof layers

$$\frac{dT_{mor,2,zi}}{dt} = \frac{A_{r,zi}}{C_{mor,2,zi}} [U_{mor1,mor2}(T_{mor,1,zi} - T_{mor,2,zi}) - U_{mor2,crt1}(T_{mor,2,zi} - T_{crt,1,zi})] \quad (36)$$

$$\frac{dT_{crt,1,zi}}{dt} = \frac{A_{r,zi}}{C_{crt,1,zi}} [U_{mor2,crt1}(T_{mor,2,zi} - T_{crt,1,zi}) - U_{crt1,crt2}(T_{crt,1,zi} - T_{crt,2,zi})] \quad (37)$$

$$\frac{dT_{crt,2,zi}}{dt} = \frac{A_{r,zi}}{C_{crt,2,zi}} [U_{crt1,crt2}(T_{crt,1,zi} - T_{crt,2,zi}) - U_{crt2,plas}(T_{crt,2,zi} - T_{plas,zi})] \quad (38)$$

$$\frac{dT_{plas,zi}}{dt} = \frac{A_{r,zi}}{C_{plas,zi}} [U_{crt2,plas}(T_{crt,2,zi} - T_{plas,zi}) - U_{plas,z}(T_{plas,zi} - T_{zi})] \quad (39)$$

By using these nodal surface temperatures, and assuming that the zone air is well mixed, the energy and humidity ratio balance equations for each zone were derived. These equations are

$$C_{zi} \frac{dT_{zi}}{dt} = \sum_{j=S,N,E,W} [U_{plas,z} A_{w,zi,j} (T_{plas,zi,j} - T_{zi})] + U_{plas,z} A_{r,zi} (T_{plas,zi} - T_{zi}) + \sum_{j=S,N,E,W} [U_{win} A_{win,zi,j} (T_o - T_{zi}) + A_{win,zi,j} I_{solar,j} SC] + Q_{occu,zi} + Q_{l,zi} + Q_{eq,zi} + \frac{ACH}{3600} V_{zi} \rho_a (T_o - T_{zi}) - U_{asp,zi} \dot{m}_{aspd,zi} c_a (T_{zi} - T_{asp,zi}) \quad (40)$$

$$W_{zi} = \frac{\frac{ACH}{3600} V_{zi} \rho_a (W_o - W_{zi}) + N_{occu,zi} \dot{W}_{occu,zi} CLF_{occu,zi}}{U_{asp,zi} \dot{m}_{aspd,zi}} + W_{asp,zi} \quad (41)$$

$$RH_{zi} = \frac{W_{zi}}{W_{sat@T_{zi}}} * 100\% \quad (42)$$

where $U_{asp,zi}$ is the supply airflow rate for zone i , which is used to control the zone i air temperature T_{zi} . These model equations are used to calculate the zone air temperature, the humidity ratio, and the relative humidity of each zone.

9.1 Simulation of IB-HVAC system

A two-floor commercial building (65 m (L) × 56 m (W) × 4 m (H)) located in Montreal was considered for simulating the IB-HVAC system. The 1st floor of the building is considered zone-1, and the 2nd floor is considered zone-2. Each zone has its own air handling unit (AHU) that receives chilled water from the centrifugal chiller system. The air is conditioned and supplied to each zone. The cooling load due to heat gains from the

Table 1 IB-HVAC system design and operating parameters

Variable	Range
Building location	Montreal Lat.45.5 N
Two-story building	Each floor, 65 m L×56 m W×4 m H
Zone-1 occupied hours and set-point	9:00–18:00; 23 °C
Zone-2 occupied hours and set-point	8:00–22:00; 24 °C
Zone-1 supply air temperature setpoint	13 °C
Zone-2 supply air temperature setpoint	14 °C
Unoccupied hours setpoint	27 °C
Relative humidity occupied periods	40–45% RH
AHU-1 capacity	75 tons; 16,000 L/s
AHU-2 capacity	80 tons; 17,000 L/s
Occupancy	7–50 per 100 m ²
Outdoor air ventilation	8–10 L/s per person
Average lighting loads	10–20 watts per m ²
Average equipment loads	20–50 watts per m ²
Air infiltration	0.25–0.5 air changes per hour
Centrifugal chiller capacity	190 tons
Cooling tower capacity	250 tons

walls, roof, windows, occupants, lighting systems, equipment, infiltration, and fresh air was calculated by solving the model Eqs. (32–42) and using the guidelines described in the ASHRAE Cooling and Heating load Calculation Manual [13]. The building operating conditions

and the capacities of the AHUs, centrifugal chiller, and the cooling tower used in the simulation tests are listed in Table 1.

9.2 Overall control structure of the IB-HVAC system

The complete control structure of IB-HVAC system with the NAPI chiller control is depicted in Fig. 9. The figure shows eight control loops, including the three chiller control loops. Since the chiller operates in full load and partial load conditions during a typical day, the chiller control includes all three control loops namely, compressor speed control, IGV control, and liquid level control loops. The NAPI is applied to compressor speed control. The remaining control loops have constant gain PI controllers, and their PI constants were obtained by using Ziegler-Nichols tuning rules [1]. The integrated system was operated over a typical day. Under this scenario, the chiller operates either in speed control mode or IGV control mode as a function of load. A control mode selector switch activates the speed control mode or the IGV control mode according to cooling load acting on the system. In the speed control mode, the compressor speed is controlled by the NAPI controller to maintain the chilled water supply temperature at its setpoint. In the IGV control mode, the IGV position is controlled by a PI controller to maintain the chilled water supply temperature at its setpoint.

As shown in Fig. 9, each zone has its own air handling unit. The temperature of supply air is controlled by

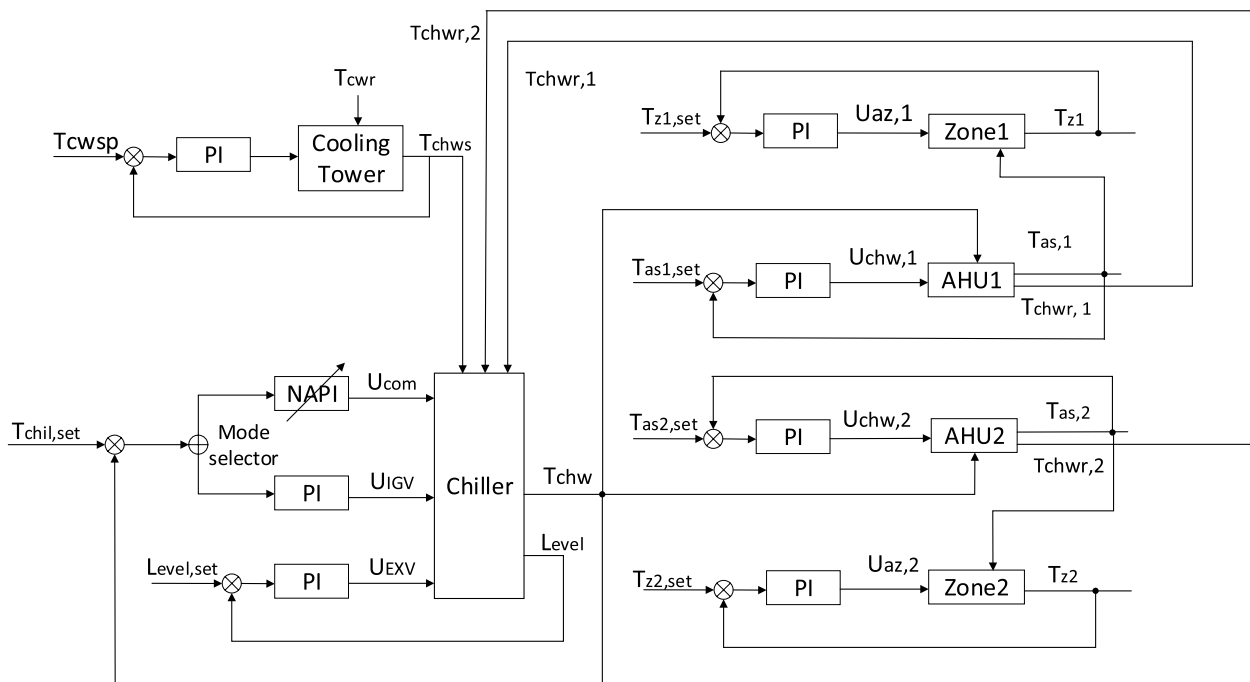


Fig. 9 Control diagram of IB-HVAC system

modulating the chilled water flow rate to the cooling coil in the air handling unit, and the air flow rate is controlled via damper control at the zone level to maintain zone air temperature at its setpoint. The interactions among the control loops are depicted by interconnecting the appropriate outputs to respective control loops. The NAPI controller now must learn and adapt to the new dynamics of the IB-HVAC system and the five additional control loops that were not part of the system when it was initially trained. The operation of this IB-HVAC system is simulated by solving the model Eqs. (1–42), and the control performance of the overall system is evaluated by conducting two sets of simulation tests. In the first test, a typical day operation of the IB-HVAC system was simulated. In the second test, a timed shutdown of one of the AHUs, indicating an equipment failure condition, was simulated, and its impact on the control of IB-HVAC system was examined.

9.3 Simulation test-1: A typical day operation of IB-HVAC system with NAPI chiller controller

In a typical day operation of IB-HVAC system, the chiller operates under variable load conditions. Therefore, the proposed neural network adaptive PI control strategy will be tested under a typical day-building operation schedule. The model Eqs. (1–42) with the eight feedback control loops shown in Fig. 9 were solved subject to outdoor weather data (Fig. 10) and the operating conditions listed in Table 1. The simulation results are plotted in Fig. 11a–v. The NAPI controller working in online mode adapts to the new system configuration and tracks the setpoints throughout the day in the presence of load changes and time-scheduled changes in setpoints. During the simulation, the chilled water temperature was maintained at 6.67 °C. The zone-1 air temperature setpoint was 23/27 °C during the occupied/unoccupied periods, while the zone-2 air temperature setpoint was 24/27 °C. The supply

air temperature to zone-1 and zone-2 was maintained at 13 and 14 °C, respectively.

The sets of Fig. 11c, g, h show the time-of-day responses of the compressor speed, liquid level, and expansion valve position due to time-varying cooling loads acting on the system. As the cooling load increases in the afternoon hours, the NAPI controller increases the compressor speed to maintain the chilled water supply temperature at its setpoint (Fig. 11d). Likewise, the AHU-1 and zone-1 temperature responses are tracking their respective setpoints shown in Fig. 11i–l.

A change in zone temperature setpoint from 27 °C during the unoccupied period to 23 °C during the occupied period causes a momentary overshoot in supply air temperature (Fig. 11l), but it reaches its setpoint shortly thereafter. Similar trends in AHU-2 and zone-2 temperature and control input responses subject to cooling loads acting on zone-2 are depicted in Fig. 11m–r. These figures also show the relative humidity responses of zone 1 and 2 (Fig. 11q). Furthermore, it is worth noting that the compressor was operating in speed control mode during the occupied period 09:00–22:00 h and in the IGV control mode during the unoccupied period spanning remainder of the day. This can be noted from Fig. 11c, t in that the IGV is fully open, and compressor speed is modulated during the occupied period (Fig. 11c), whereas IGV is modulated (Fig. 11t) while holding the compressor speed constant at surge speed during the unoccupied period.

In terms of the tracking performance of the NAPI controller, it can be noted from Fig. 11d that the chilled water supply temperature setpoint is tracked with near-zero error during the period 9:00~22:00, but during the remainder of the simulation period, there is a small difference between the controlled variable and its setpoint. The reason for that is, during the period 9:00~22:00, the centrifugal compressor is operating under speed

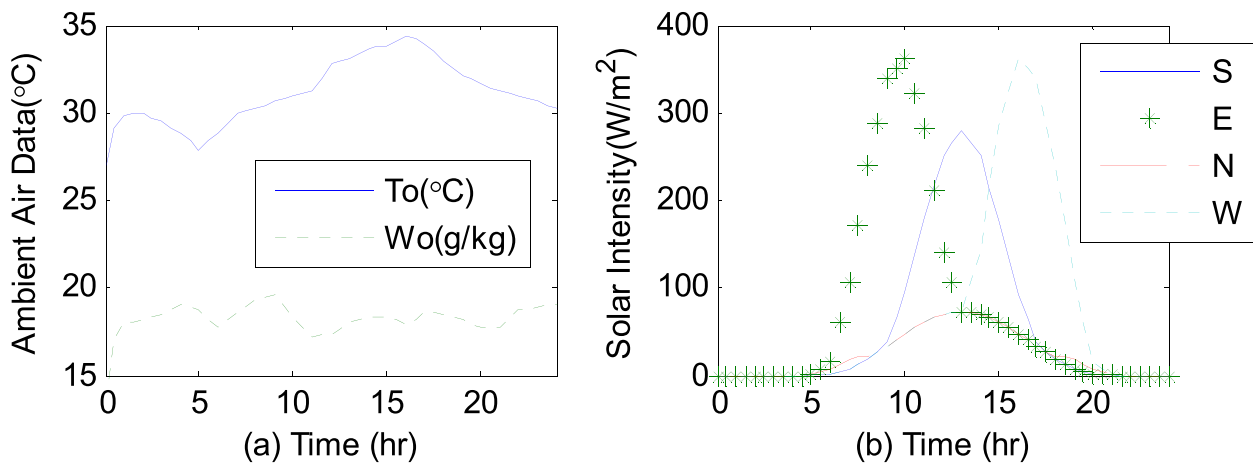


Fig. 10 Typical day weather data for Montreal

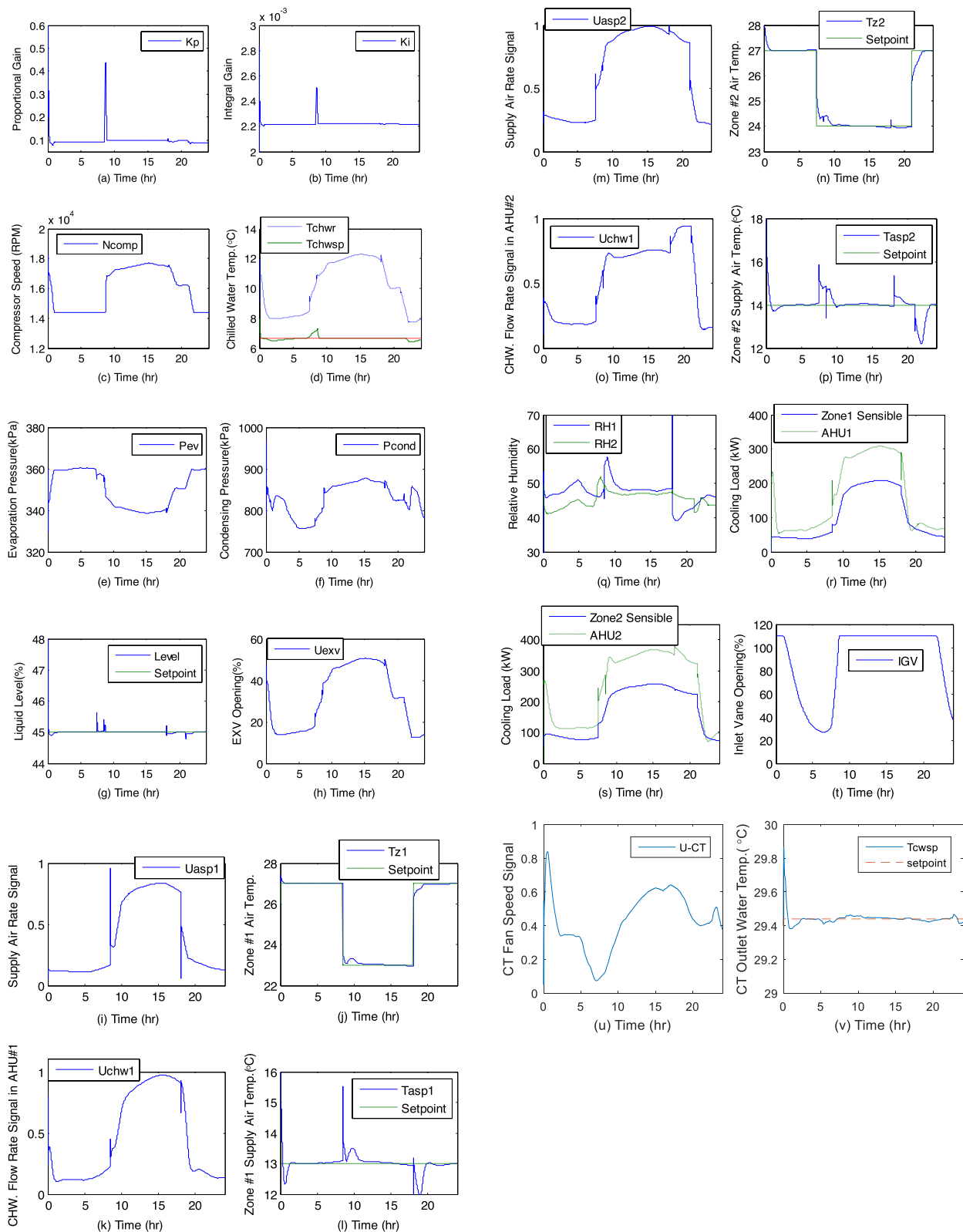


Fig. 11 a–v Closed-loop responses of the NAPI controller under a typical day IB-HVAC system operation

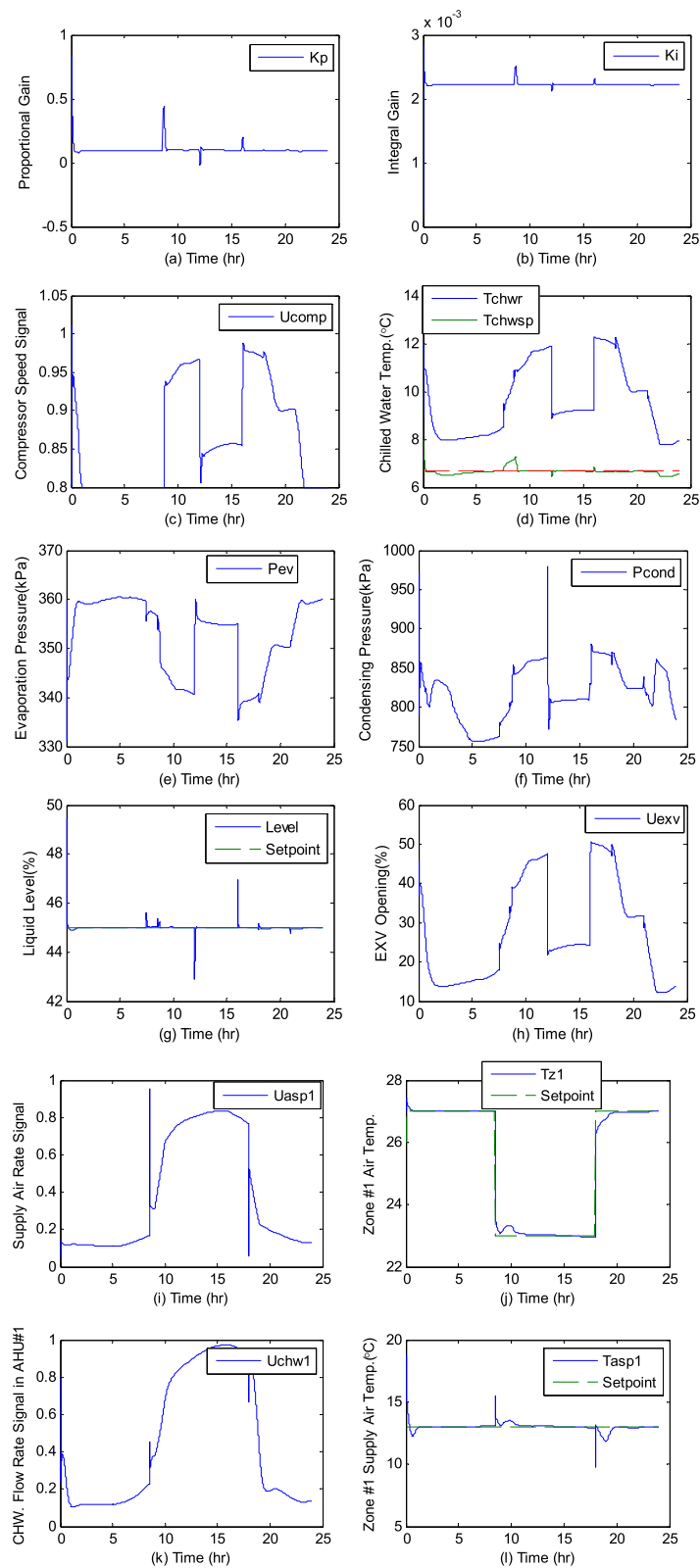


Fig. 12 a–l Responses of the NAPI controller with a sudden change in cooling loads

control mode, in which the NAPI control strategy is used to determine the input signal for compressor speed which gave near-zero tracking error; whereas during the remainder of the day, the compressor is operated under IGV control mode due to partial load conditions in which the IGV position is modulated by a constant gain PI controller that contributed to the tracking error. Figure 11u and v demonstrate the tracking performance of the cooling tower fan speed controller to maintain the cooling water supply temperature at its setpoint.

It can be concluded that the proposed NAPI control strategy is effective under different operating conditions that occur during a typical day-building operation. The time-of-day variations in cooling loads are gradual as shown in Fig. 11d, r, and s, except when a setpoint change is applied.

9.4 Simulation test-2: NAPI control performance with a large step change in cooling load due to equipment failure

Exceptionally, a building could experience a sudden decrease in cooling load due to equipment failure or safety shutdown. This scenario was simulated by turning off the zone-2 AHU-2 (Fig. 9) at 12:00 h and turning it back on 4 h later at 16:00 h. It is of interest to evaluate the impact of a sudden change in cooling load on the performance of the NAPI-controlled chiller system and to examine how the neighboring zone-1 temperature responses are affected. The closed-loop system responses obtained during this simulation test are depicted in Fig. 12a–l.

The impact of turning off the AHU-2 at 12:00 noon and turning on at 16:00 h can be observed from Fig. 12c. The compressor speed control input abruptly drops at 12:00 noon (AHU-2 shutdown) and increases to higher value as the AHU-2 is turned on at 16:00 h. From Fig. 12d, it can be observed that the NAPI controller is able to maintain the chilled water supply temperature $T_{chw,sp}$ at its setpoint. Although a significant decrease in cooling load occurs at 12:00 h, the chiller output response is not significantly affected. This is because the NAPI controller adapts to load changes and takes prompt action by adjusting the proportional and integral gains (Fig. 12a, b) to provide smooth and stable response. Likewise, when the cooling load is restored back at 16:00 h, at which point the chiller load encounters sudden increase in the cooling load, there is also very little adverse impact as the NAPI controller quickly restores the system output to maintain stable and smooth responses. The $T_{chw,sp}$ response showed about 3% overshoot and took 30–45 min to reach the setpoint. Also, from Fig. 12j, it can be noted that zone-1 temperature responses remained close to its setpoint showing only slight overshoot at the time of sudden change in cooling load. From the simulation results,

it is concluded that the proposed online adaptive control strategy responds well to significant changes in cooling loads and, thus, is a suitable choice for practical applications in centrifugal chiller systems.

10 Summary and conclusions

A neuro-adaptive control strategy for speed control of a centrifugal chiller system is developed, and its control performance is tested via simulations under a wide range of operating conditions. A 3–2–1-layer neural network adaptive PI controller is designed in which the controller gains are updated online by optimization of network weights. The controller gains are obtained from the outputs of the hidden layer.

Simulation results show that compared to the constant gain PI control, the neuro-adaptive PI control gives near-zero setpoint tracking and smooth control over a wide range of operating conditions. The constant gain PI controller responses for chilled water supply temperature showed 1.5% overshoot, 1-h steady-state time and 1% steady-state setpoint tracking error. On the other hand, the responses of the NAPI controller under the same operating conditions showed slightly higher overshoot (3%), faster steady-state time (30 min), and zero steady-state setpoint tracking error.

The neuro-adaptive controller is found to give robust control performance when subjected to unseen system operating conditions in an integrated building and HVAC system and consequently multiple load changes acting simultaneously from different components of the integrated system. It was found that a 50% change in cooling load and a 4 °C change in zone temperature setpoint had very little impact on the NAPI controller performance. The overshoot remained below 3% with 30–45 min steady-state time. The neuro-adaptive controller is shown to perform well in a hybrid control structure involving multiple PI controllers in the IB-HVAC system during a typical day operating condition.

Abbreviations

Nomenclature

a	Acoustic velocity at the impeller inlet
$A_{EXV,max}$	Maximum opening area of the EXV, m ²
C	Thermal capacity, J/K
C_d	Discharge coefficient of the expansion valve
cf	Cooling factor for the compressor motor
c_w	Specific heat of the water, J/(kg K)
D	Diameter of the compressor impeller, m
L	Length of the evaporator vessel or condenser vessel, m
g	Gravitational acceleration, m/s ²
h	Rise in pressure head of the refrigerant across the compressor, m
h_{fg}	Enthalpy change per unit mass of refrigerant due to phase change, J/kg
h_{re}	Enthalpy of the refrigerant, J/kg
L_{level}	Refrigerant liquid level in the condenser

$LMTD$	Log-mean temperature difference between the water and the refrigerant, °C
\dot{m}	Mass flow rate of the fluid, kg/s
$m_{0,c}$	Initial mass of the refrigerant in the condenser at the chiller starting point, kg
$m_{re,c}$	Total mass of the refrigerant in the condenser, kg
$m_{re,charge}$	Total mass of the refrigerant charged in the chiller, kg
$\dot{m}_{re,comp}$	Refrigerant mass flow rate compressed by the compressor, kg/s
$\dot{m}_{re,ev}$	Refrigerant vapor generation rate in the evaporator, kg/s
$\dot{m}_{re,EXV}$	Refrigerant mass flow rate through the electronic expansion valve, kg/s
$m_{re,motor}$	Refrigerant mass flow rate used to cool the compressor motor, kg/s
n	Polytropic index
$N_{com,max}$	Maximum rotational speed of the compressor, rpm
N_{tb}	Number of copper tubes
P_c	Condensing pressure, kPa
P_{elec}	Electrical power consumption by the compressor, kW
P_{ev}	Evaporation pressure, kPa
PLR	Partial load ratio
ΔP_{re}	Pressure rise of the refrigerant across the compressor, m
\dot{Q}	Volumetric flow rate, m ³ /s
\dot{Q}_{motor}	Heat generation rate of the compressor, W
t	Time, s
T	Temperature, °C
T_{re}	Refrigerant temperature, °C
U	Overall heat transfer coefficient between the water and the refrigerant per unit length of copper tube, W/°C
U_{IGV}	Inlet guide vane opening position
U_{EXV}	Electronic expansion valve opening position
U_{com}	Compressor rotational speed signal
$U_{chw,s}$	Chilled water mass flow rate control input signal
U_{as}	Airflow rate control input signal
v_{disc}	Specific volume of the refrigerant vapor at the compressor discharge, kg/m ³
V_{ev}	Total volume of the shell side in the evaporator, m ³
$V_{L,c}$	Total volume of the liquid refrigerant and saturated mixture, m ³
V_p	Tip speed of the compressor impeller, m/s
V_{re}	Volume flow rate of the refrigerant, m ³ /s
$V_{tp,ev}$	Total refrigerant volume of the two-phase section, m ³
W_P	Polytropic work input per unit mass of refrigerant, kW/kg
W	Humidity ratio kg _m /kg _a
x_v	Ratio of the vapor refrigerant mass to the total refrigerant mass in the mixture before entering the evaporator

Greek letters

$\bar{\gamma}_v$	Average volume fraction of the vapor refrigerant in the TP section
ρ_{re}	Density of the refrigerant, kg/m ³
β	Angle of the impeller, rad
γ	Specific heat ratio of the refrigerant
η_P	Polytropic efficiency
η_{motor}	Compressor motor efficiency
ω	Normalized inlet guide vane opening position
μ	Compressor overall work coefficient
Θ	Percent volumetric flow
Ω	Percent head

Subscripts

1	1St section
2	2Nd section
a	Air
ACH	Air change rate

AHU	Air handling unit
c	Condenser
cw	Cooling water
chw	Chilled water
EXV	Electronic expansion valve
i	Indoor
imp	Impeller
o	Outdoor
out	Outlet
r	Return water
re	Refrigerant
satv	Saturated refrigerant vapor
satl	Saturated refrigerant liquid
sc	Sub-cool section
sh	Superheat section
sp	Supply water
suc	Suction side of the compressor
total	The total number of copper tubes
tp	Two-phase section
Z	Zone

Acknowledgements

Research funding (DG 036380) for this project from the Natural Sciences and Engineering Research Council of Canada (NSERC) is gratefully acknowledged.

Authors' contributions

M.Z. has contributed to model and control algorithm conceptualization, formal analysis of the results, validation, manuscript preparation and project supervision. S.L. has contributed to developing model equations, performing MATLAB simulations, formal analysis and corrections, figures and visualization, manuscript preparation.

Availability of data and materials

Data sharing is not applicable to this article as no datasets were generated or analyzed during the current study. equations, performing MATLAB simulations, formal analysis and corrections, figures and visualization, manuscript

Declarations**Competing interests**

The authors declare that they have no competing interests.

Received: 3 August 2023 Accepted: 5 August 2024

Published online: 04 September 2024

References

- Astrom, K. J., & Hagglund, T. (1995). *PID controllers: Theory, design and tuning*. Instrument Society of America.
- Li, L., & Zaheeruddin, M. (2007). Hybrid fuzzy logic control strategies for hot water district heating systems. *Building Services Engineering Research and Technology*, 28(1), 1–35.
- Pal, A., & Mudi, R. K. (2008). Self-tuning fuzzy PI controller and its application to HVAC systems. *International Journal of Computational Cognition*, 6(1), 25–30.
- Wu, J., & Cai, W. (2000). *Development of an adaptive neuro-fuzzy method for supply air pressure control in HVAC system. Smc 2000 conference proceedings*. 2000 IEEE international conference on Systems, Man & Cybernetics.
- Zaheeruddin, M., & Tudoroiu, N. (2004). Neuro-PID tracking control of a discharge air temperature system. *Energy Conversion and Management*, 45, 2405–2415.
- Ning, M. (2008). *Neural network based optimal control of HVAC&R systems, PhD thesis Department of Building, Civil and Environmental Engineering*. Montreal, Quebec: Concordia University.
- Zeng, S., Hu, H., Xu, L., & Li, G. (2012). Nonlinear adaptive PID control for greenhouse environment based on RBF network. *Sensors*, 12, 5328–5348.

8. Rasmussen, B., & Alleyne, A. (2006). *Dynamic modeling and advanced control of air conditioning and refrigeration systems*. Air Conditioning and Refrigeration Center TR-244.
9. Oliveira, V., Trofino, A., & Hermes, C. (2011). A switching control strategy for vapor compression refrigeration systems. *Applied Thermal Engineering*, 31, 3914–3921.
10. Sun, Y., Wang, H., & SG. (2009). Chiller sequencing control with enhanced robustness for energy efficient operation. *Energy and Buildings*, 41, 1246–1255.
11. Chang, Y. C. (2006). An outstanding method for saving energy-optimal chiller operation. *IEEE Transactions on Energy Conversion*, 21(2), 527–532.
12. Li, S., & Zaheeruddin, M. (2019). Dynamic modelling and multi-mode control of a centrifugal chiller system: A computer simulation study. *Int J Air-conditioning and Refrigeration*, 27(4), 1950031.
13. ASHRAE. (1992). *ASHRAE cooling and heating load calculation manual*, Atlanta, U.S.A.
14. Korpela, S. A. (2011). *Principles of turbomachinery*. John Wiley & Sons Inc.
15. Bendapudi, S., Braun, J. E., & Groll, E. A. (2005). Dynamic model of a centrifugal chiller system-model development, numerical study, and validation. *ASHRAE Transactions*, 111, 132–147.
16. Wong, S. P. W., & Wang, S. K. (1989). System simulation of the performance of a centrifugal chiller using a shell-and-tube-type water-cooled condenser and R-11 as refrigerant. *ASHRAE Transaction*, 95(1), 445–454.
17. Yu, F. W., & Chan, K. T. (2006). Improved condenser design and condenser-fan operation for air-cooled chillers. *Applied Energy*, 83, 628–648.

Publisher's Note

Springer Nature remains neutral with regard to jurisdictional claims in published maps and institutional affiliations.